

Modeling the Anisotropic Tidal Effect on the Spin-Spin Correlations of Low-Mass Galactic Halos

Jounghun Lee

*Astronomy Program, Department of Physics and Astronomy, Seoul National University,
Seoul 08826, Republic of Korea*

jounghun@astro.snu.ac.kr

ABSTRACT

The halo spin-spin correlation function, $\eta(r)$, measures how rapidly the strength of the alignments of the spin directions between the neighbor halos change with the separation distance, r . The previous model based on the tidal torque theory expresses the halo spin-spin correlation function as a power of the linear density two-point correlation function, $\eta(r) \propto \xi^n(r)$, predicting $n = 2$ in the linear regime and $n = 1$ in the non-linear regime. Using a high-resolution N-body simulation, we show that the halo spin-spin correlation function in fact drops much less rapidly with r than the prediction of the previous model, finding $\eta(r)$ to be statistically significant even at $r \geq 10 h^{-1} \text{Mpc}$ on the dwarf galaxy scale. Claiming that the anisotropic tidal effect is responsible for the failure of the previous model, we propose a new formula for the halo spin-spin correlation function expressed in terms of the integrals of $\xi(r)$. The new formula with the best-fit parameters turns out to agree excellently with the numerical results in a broad mass range, $0.05 \leq M/(10^{11} h^{-1} M_{\odot}) \leq 50$, describing well the large-scale tail of $\eta(r)$. We discuss a possibility of using the large-scale spin-spin correlations of the dwarf galactic halos as a complementary probe of dark matter.

Subject headings: cosmology:theory — large-scale structure of universe

1. Introduction

One of the main missions of modern cosmology is to determine the initial conditions of the universe from the observables. For the completion of this mission, such linear observables as the cosmic microwave background radiation (CMB), large scale velocity flows, baryonic acoustic oscillations (BAO) and etc., which do not evolve much from the initial

states and thus can be well described by the first order perturbation theory, have been regarded as the most optimal diagnostics (e.g., Vittorio et al. 1986; de Bernardis et al. 2000; Seo, & Eisenstein 2003). Powerful as they are as a probe of cosmology, the simultaneous dependence of these linear observables on the multiple parameters that are required to describe the cosmological initial conditions often invokes the degeneracy problem. For example, it was recently shown by Park, & Ratra (2018) that although the Planck satellite experiment advocates a flat Λ CDM universe whose energy density is dominated by the cosmological constant Λ and cold dark matter (CDM) with zero spatial curvature (Planck Collaboration et al. 2014), a non-flat Λ CDM universe fits the CMB and BAO data on the large-scale equally well if the Hubble constant, H_0 , has a much lower value than the Planck best-fit result.

Prospecting the near-field non-linear observables for complementary cosmological probes has been on the rise to overcome the limitations of the linear counterparts, in spite of their complicated nature that often defies any analytical approaches (Bland-Hawthorn, & Peebles 2006). Given the high-energy physics often leave imprints on the small-scales (for a review, see Biagetti 2019), it was suggested that a prominent diagnostics based on the non-linear observables, if found, should enable us not only to break the parameter degeneracy but also to open a new window on the early universe. Among various nonlinear observables suggested so far as probes of cosmology such as the compact mini-halos, dynamics of the Local Group, wide binary stars, velocity distribution function of galaxy clusters, properties of neutron stars, and so on (e.g., Aslanyan et al. 2016; Carlesi et al. 2017; Ntampaka et al. 2017; Banik, & Zhao 2018; Silva, & Yunes 2019), the galaxy spin-spin correlation function has recently garnered astute attentions because of its good prospects for the practical application. For instance, Schmidt et al. (2015) claimed that the anisotropic inflation models can be tested and constrained by measuring the galaxy shape-shape (or spin-spin) correlation function (see also Chisari et al. 2016; Kogai et al. 2018). Very recently, Yu et al. (2019) found it possible in principle to detect a signal of the spontaneous breaking of chiral symmetry predicted by the quantum chromodynamics from the measurement of the galaxy spin-spin correlation function.

Constructing a solid theoretical framework for the galaxy spin-spin correlation function is a prerequisite toward its success as a probe of cosmology. It was Pen et al. (2000) who for the first time developed an analytic formula for the galaxy spin-spin correlation function, $\eta(r)$, based on the linear tidal torque theory (Doroshkevich 1970; White 1984), according to which $\eta(r)$ is proportional to the square of the linear density two-point correlation function, $\xi^2(r)$. Their model, however, turned out to fail in matching on a quantitative level the numerical results from N-body simulations in which $\eta(r)$ was found to drop with r not so rapidly as $\xi^2(r)$. Ascribing this disagreement to the development of the non-Gaussianity of the tidal fields in the non-linear regime, Hui & Zhang (2002) claimed that $\eta(r)$ in the

nonlinear regime should be described as a linear scaling of $\xi(r)$ (see also Hui, & Zhang 2008). Their claim of $\eta(r) \propto \xi(r)$ was later confirmed by Lee & Pen (2008) at low-redshifts ($z \leq 0.5$) in the halo mass range of $10^{11} \leq M/(h^{-1} M_{\odot}) \leq 10^{13}$.

Although the linear scaling of $\eta(r)$ with $\xi(r)$ was found to work quite well at distances of $r < 10 h^{-1}\text{Mpc}$, it turned out to fail in describing the tail of $\eta(r)$ at larger distances $r \geq 10 h^{-1}\text{Mpc}$ (Lee & Pen 2008). Moreover, this model has an conceptual downside: the anisotropic tidal effect has not been properly taken into account, which is likely to be the cause of its failure at $r \geq 10 h^{-1}\text{Mpc}$. Among many aspects of the evolved tidal fields, it should not be only the non-Gaussianity that leads the spin-spin correlation function to decrease slowly with r . As a matter of fact, the growth of the anisotropy in the evolved tidal fields may contribute even more to the generation of the galaxy spin-spin correlation at large scales, given the recent numerical finding that the cosmic web generated by the anisotropic tidal fields are closely linked with the intrinsic spin alignments of the low-mass galaxies (Codis et al. 2015a). In this Paper, we attempt to find a new improved formula for $\eta(r)$ that is valid at larger distances even on the dwarf galaxy scale by taking the anisotropic tidal effects into consideration. Our analysis will be done in the framework of the extended model for the tidally induced spin alignments recently proposed by Lee (2019) to describe the intrinsic alignments between the directions of the galaxy spins (and shapes) and the eigenvectors of the local tidal tensors.

The outlines of the upcoming Sections are as follows. Section 2.1 is devoted to reviewing the extended model for the tidally induced spin alignments on which a new formula for $\eta(r)$ will be based. Section 2.2 is spared to prove the validity of the extended model for the tidally induced spin alignment on the dwarf galaxy scale. Section 3.1 is devoted to reviewing the previous models for the spin-spin correlation functions and to explaining their limitations as well as their merits. Section 3.2 presents a new formula for the galaxy spin-spin correlation function based on the extended model for the tidally induced spin alignments. Section 3.3 is spared to show how successfully the new formula for the galaxy spin-spin correlation function survives a numerical test in a broad mass range at various redshifts. The summary of our achievements and the discussion of the future application of our new model are presented in Section 4.

2. Tidally Induced Spin Alignments on the Dwarf Galaxy Scales

2.1. Review of the Analytic Framework

Throughout this Paper, we will let the unit spin vector of a dark matter halo, unit traceless tidal tensor surrounding a halo, set of three eigenvalues of the unit traceless tidal tensor in a decreasing order and set of the corresponding tidal eigenvectors be denoted by $\hat{\mathbf{s}} = (\hat{s}_i)$, $\hat{\mathbf{T}} = (\hat{T}_{ij})$, $\{\hat{\lambda}_1, \hat{\lambda}_2, \hat{\lambda}_3\}$ and $\{\hat{\mathbf{p}}_1, \hat{\mathbf{p}}_2, \hat{\mathbf{p}}_3\}$, respectively. We will also let s , M and R_f denote the magnitude of the spin vector, halo mass, and smoothing scale, respectively.

The original model developed by Lee & Pen (2000) for the tidally induced spin alignments of dark matter halos assumes that the conditional probability density function, $p(s, \hat{\mathbf{s}}|\hat{\mathbf{T}})$, follows a multi-variate Gaussian distribution, and that the conditional covariance, $\langle \hat{s}_i \hat{s}_j | \hat{\mathbf{T}} \rangle$, can be expressed in terms of the anti-symmetric product of $\hat{\mathbf{T}}$ as

$$\langle \hat{s}_i \hat{s}_j | \hat{\mathbf{T}} \rangle = \left(\frac{1}{3} + \frac{3}{5} c_t \right) \delta_{ij} - \frac{3}{5} c_t \hat{T}_{ik} \hat{T}_{kj}, \quad (1)$$

where c_t , called the spin correlation parameter, ranges from 0 to 1. Equation (1) provides the simplest description of the $\hat{\mathbf{s}}\text{-}\hat{\mathbf{p}}_2$ alignment whose presence was naturally predicted by the linear tidal torque theory (Doroshkevich 1970; White 1984) but whose strength cannot be determined from the first principle due to its stochastic nature (Lee & Pen 2000; Porciani et al. 2002).

Rearranging the terms in Equation (1) about c_t in the principal frame of $\hat{\mathbf{T}}$ gives

$$c_t = 10 \left(\frac{1}{3} - \sum_{i=1}^3 \hat{\lambda}_i^2 \hat{s}_i^2 \right), \quad (2)$$

which translates a larger value of c_t into a stronger $\hat{\mathbf{s}}\text{-}\hat{\mathbf{p}}_2$ alignment. Before the turn-around moment when $(s, \hat{\mathbf{s}})$ continues to grow under the influence of $\hat{\mathbf{T}}$, c_t will increase with time. At the turn-around moment when c_t reaches the maximum value of unity, the tidal interaction between $\hat{\mathbf{T}}$ and $\hat{\mathbf{s}}$ will be terminated. After the turn-around moment when both of $\hat{\mathbf{T}}$ and $\hat{\mathbf{s}}$ grow nonlinearly, being decoupled from each other, c_t would gradually diminish from unity. Therefore, the spin correlation parameter, c_t , is expected to depend on M and z , having lower values for the case of lower-mass halos at lower redshifts, which must have turned around at earlier epochs.

Multiple N-body simulations limited the validity of Equation (1) to $M \geq M_c$ with $M_c \approx 5 \times 10^{12} h^{-1} M_\odot$ (Aragón-Calvo et al. 2007; Hahn et al. 2007; Paz et al. 2008; Zhang, Yang & Faltenbacher 2009; Codis et al. 2012; Libeskind et al. 2013; Trowland et al. 2013; Ganeshiah Veena et al.

2018), demonstrating that the halos with $M < M_c$ exhibit the $\hat{\mathbf{s}}\text{-}\hat{\mathbf{p}}_3$ rather than $\hat{\mathbf{s}}\text{-}\hat{\mathbf{p}}_2$ alignment. Although much effort was made to explain this *spin flip* phenomena, it has yet to be fully understood what the physical meaning of M_c is (Bett & Frenk 2012; Lacerna & Padilla 2012; Codis et al. 2012; Libeskind et al. 2013; Welker et al. 2014; Codis et al. 2015b; Laigle et al. 2015; Bett & Frenk 2016; Ganeshiaiah Veena et al. 2018).

In line with this effort, Lee (2019) recently put forth an *extended model for the tidally induced spin alignments* by adding to Equation (1) a new term proportional to $\hat{\mathbf{T}}$ in order to describe the change of the alignment tendency between $M < M_c$ and $M \geq M_c$.

$$\langle \hat{s}_i \hat{s}_j | \hat{\mathbf{T}} \rangle = \left(\frac{1}{3} + \frac{3}{5}c_t + \frac{3}{5}d_t \right) \delta_{ij} - \frac{3}{5}c_t \sum_{k=1}^3 \hat{T}_{ik} \hat{T}_{kj} - \frac{3}{5}d_t \hat{T}_{ij}, \quad (3)$$

where an additional parameter (called the second spin correlation parameter), d_t , ranging from 0 to 1, is introduced to quantify the $\hat{\mathbf{s}}\text{-}\hat{\mathbf{p}}_3$ alignment.

Lee (2019) derived a formula for d_t in terms of $(\hat{\lambda}_i)$ and (\hat{s}_i) from Equation (3) as

$$d_t = \frac{3}{5} \sum_{i=1}^3 \hat{\lambda}_i \hat{s}_i^2, \quad (4)$$

which translates a larger value of d_t into a stronger $\hat{\mathbf{s}}\text{-}\hat{\mathbf{p}}_3$ alignment. It was also shown by Lee (2019) that the value of d_t obtained by Equation (4) increases as M decreases and that the ratio of d_t to c_t reaches unity at a certain mass scale which turns out to be quite close to the critical mass scale for the spin flip phenomenon, M_c .

Lee (2019) derived three probability density functions, $p(|\hat{\mathbf{s}} \cdot \hat{\mathbf{p}}_1|)$, $p(|\hat{\mathbf{s}} \cdot \hat{\mathbf{p}}_2|)$, $p(|\hat{\mathbf{s}} \cdot \hat{\mathbf{p}}_3|)$, based on this model,

$$p(|\hat{\mathbf{p}}_i \cdot \hat{\mathbf{s}}|) = \frac{1}{2\pi} \int_0^{2\pi} \left[\prod_{n=1}^3 \left(1 + c_t - 3c_t \hat{\lambda}_n^2 + d_t - 3d_t \hat{\lambda}_n \right) \right]^{-\frac{1}{2}} \times \left[\sum_{l=1}^3 \left(\frac{|\hat{\mathbf{s}} \cdot \hat{\mathbf{p}}_l|}{1 + c_t - 3c_t \hat{\lambda}_l^2 + d_t - 3d_t \hat{\lambda}_l} \right) \right]^{-\frac{3}{2}} d\phi_{jk}. \quad (5)$$

where ϕ_{jk} is the azimuthal angle defined in the plane normal to $\hat{\mathbf{p}}_i$, and proved that all of them were in excellent simultaneous agreement with the numerical results without resorting to any fitting procedure, provided that M is in the range of $0.5 \leq M/(10^{11} h^{-1} M_\odot) \leq 50$ and $\hat{\mathbf{T}}$ smoothed on the scales of $R_f \geq 5 h^{-1} \text{Mpc}$. Moreover, it was also shown that Equation (5) naturally predicts the $\hat{\mathbf{s}}\text{-}\hat{\mathbf{p}}_2$ alignment for the case of $M \geq M_c$, the $\hat{\mathbf{s}}\text{-}\hat{\mathbf{p}}_3$ alignment for the case of $M < M_c$ and the $\hat{\mathbf{s}}\text{-}\hat{\mathbf{p}}_1$ anti-alignment for both of the cases (Lee 2019).

2.2. Extension to the Dwarf Galaxy Scales

Now, we would like to investigate whether or not the extended model for the tidally induced spin alignments is also valid for the lower-mass halos with $M < 5 \times 10^{10} h^{-1} M_{\odot}$ in the highly nonlinear regime. For this investigation, we utilize a dataset from the ν^2 GC-H2 (New Numerical Galaxy Catalog) simulation conducted by Ishiyama et al. (2015) for the Planck cosmology. The linear box size (L_{box}), total number of DM particles (N_{tp}), mass resolution (m_{dm}) of the ν^2 GC-H2 simulations are as follows: $L_{\text{box}} = 70 h^{-1} \text{Mpc}$, $N_{\text{tp}} = 2048^3$ and $m_{\text{dm}} = 3.44 \times 10^6 h^{-1} M_{\odot}$. The ν^2 GC-H2 simulation provides the friends-of-friends (FoF) group catalog as well as the Rockstar halo catalog at various snapshots. The former contains information only on the position (\mathbf{x}) and number of constituent particles (N_p) of each halo, while additional information on the spin angular momentum and virial mass of each halo is available from the latter (Behroozi et al. 2013). From the Rockstar catalog, we extract the *distinct low-mass halos* with $M \leq 5 \times 10^{10} h^{-1} M_{\odot}$ to the exclusion of those halos with $N_p < 300$ whose spin directions are likely contaminated by the poor-resolutions (Bett et al. 2007).

Applying the clouds-in-cell methods to the FoF group catalog at $z = 0$ without putting a mass-cut, we construct the density contrast field on 256^3 grid points. Then, we obtain the gravitational potential field by applying the inverse Poisson equation to the reconstructed density contrast field, convolve it with a Gaussian filter on the scale of $R_f = 0.5 h^{-1} \text{Mpc}$ (corresponding to the highly nonlinear regime), and reconstruct the tidal field by numerically calculating the second derivative of the convolved gravitational potential field. Through the interpolation of the reconstructed tidal field, we determine $\hat{\mathbf{T}}$ at the location of each halo, and then find $\{\hat{\lambda}_3\}_{i=1}^3$ and $\{\hat{\mathbf{p}}_i\}_{i=1}^3$ through a similarity transformation of $\hat{\mathbf{T}}$. For each halo, we take the absolute value of the projection of $\hat{\mathbf{s}}$ onto the i th eigenvector direction, $|\hat{\mathbf{s}} \cdot \hat{\mathbf{p}}_i|$. Dividing the range of $[0, 1]$ into multiple bins of the same length, we investigate how frequently the measured value of $|\hat{\mathbf{s}} \cdot \hat{\mathbf{p}}_i|$ falls into each bin. This frequency divided by the bin length yields the numerical result of the probability density, $p(|\hat{\mathbf{s}} \cdot \hat{\mathbf{p}}_i|)$.

Given the result of Lee (2019) that the value of c_t is negligibly small for $M \leq 10^{11} h^{-1} M_{\odot}$, we set $c_t = 0$ in Equation (5). Determining d_t by Equation (4) for each halo, we put the mean value of d_t averaged over the selected halos into Equation (5) with $c_t = 0$ to complete the analytic results. Figure 1 compares the analytically determined probability densities (brown solid lines) with the numerical results (filled circles). Note the excellent simultaneous agreements between the numerical and analytical results even though no fitting procedure is involved: the observed strong $\hat{\mathbf{s}}\text{-}\hat{\mathbf{p}}_3$ alignment, strong $\hat{\mathbf{s}}\text{-}\hat{\mathbf{p}}_1$ anti-alignment and weak $\hat{\mathbf{s}}\text{-}\hat{\mathbf{p}}_2$ anti-alignment are simultaneously well described by the analytic results, which confirms the validity of Equations (3)-(5) in the highly nonlinear regime characterized by

$M \leq 5 \times 10^{10} h^{-1} M_{\odot}$ and $R_f = 0.5 h^{-1} \text{Mpc}$.

3. A New Model for the Halo Spin-Spin Correlations

Now that the extended model for the tidally induced spin alignments are found to successfully work on the dwarf galactic scale, we would like to construct a new improved formula for the spin-spin correlations of abundant dwarf galactic halos in the framework of this model, in the hope that it could describe well the behavior of the halo spin-spin correlation function at large distances. But, before embarking on this task, we would like to briefly review the previous formulae that have paved a path to this new one.

3.1. Review of the Previous Models

Pen et al. (2000) defined the halo spin-spin correlation function, $\eta(r)$, as an ensemble average of the square of the dot product of the unit spin vectors of two galactic halos at the positions of \mathbf{x} and \mathbf{x}' , respectively, with separation distance $r \equiv |\mathbf{x} - \mathbf{x}'|$:

$$\eta(r) \equiv \langle |\hat{\mathbf{s}}(\mathbf{x}) \cdot \hat{\mathbf{s}}'(\mathbf{x}')|^2 \rangle - \frac{1}{3}. \quad (6)$$

Note that $\eta(r)$ vanishes at large r since the first ensemble average term in the right-hand side (RHS) reaches $1/3$ at large r .

Putting Equation (1) into Equation (6), Pen et al. (2000) derived the following approximate formula for $\eta(r)$ with the help of Wick's theorem under the assumption that the surrounding tidal field is Gaussian and isotropic (see also Appendix H in Lee & Pen 2001)¹.

$$\eta(r) = \frac{9}{25} c_t^2 \langle \hat{T}_{ik} \hat{T}'_{il} \hat{T}_{kj} \hat{T}'_{lj} \rangle - \frac{1}{3} \quad (7)$$

$$\approx \frac{9}{25} c_t^2 \frac{\langle \tilde{T}_{ik} \tilde{T}'_{il} \tilde{T}_{kj} \tilde{T}'_{lj} \rangle}{\langle |\tilde{T}|^2 |\tilde{T}'|^2 \rangle} - \frac{1}{3} \quad (8)$$

$$\approx a_{\text{nl}}^2 \frac{\xi^2(r)}{\sigma^2}, \quad (9)$$

where $\xi(r)$ and σ^2 are the two-point and auto correlation functions of the linear density field smoothed on R_f , respectively.

¹In Lee & Pen (2001), the spin correlation parameter a equals $3c_t/5$

The proportionality constant factor, a_{nl} , between $\eta(r)$ and the rescaled density correlation $\tilde{\xi}(r) \equiv \xi(r)/\sigma^2$ is close to $3c_t^2/50$ if the smoothing scale R_f equals the Lagrangian radius of the halo mass, R_{th} (Lee & Pen 2001). If R_f is different from R_{th} , the value of a_{nl} would differ from $3c_t^2/50$. Pen et al. (2000) treated this proportionality constant factor, a_{nl} , as an adjustable parameter, given all the uncertainties involved in the approximations made in the derivation of Equations (8)-(9) as well as the difference between R_f and R_{th} . The key prediction of Equation (9) was that as $\eta(r)$ drops with r as rapidly as $\xi^2(r)$, the halo spin-spin correlation signal should be negligibly small at distances larger than a few megaparsecs (Pen et al. 2000; Lee & Pen 2001), which was later contradicted by several numerical results (Hui & Zhang 2002; Lee & Pen 2008; Hui, & Zhang 2008).

What failed Equation (9) was not only the disagreements with the numerical results but also the limitation of its critical assumption that the tidal fields are Gaussian and isotropic. Although this simple assumption allowed the halo spin-spin correlation function to be expressed in terms of the linear observables, it was to fail for the description of the spin-spin correlation function of the galactic halos since the tidal field on the galactic scale is neither Gaussian nor isotropic. It was Hui & Zhang (2002) who pointed out the unrealistic assumption that underlies Equation (9) about the Gaussianity of the tidal fields and claimed that the growth of the non-Gaussianity would drive $\eta(r)$ to be proportional to $\tilde{\xi}(r)$ rather than $\tilde{\xi}^2(r)$, which was confirmed by the subsequent numerical work of Lee & Pen (2008).

To take into account the effect of the non-Gaussian tidal fields on the halo spin-spin correlations, Lee & Pen (2008) suggested the following simple modification of Equation (9) in the hope that it would yield a better agreement with the numerical results:

$$\eta(r) \approx a_l \tilde{\xi}^2(r) + \epsilon_{\text{nl}} \tilde{\xi}(r), \quad (10)$$

where a_l and ϵ_{nl} are two adjustable parameters. Determining the best-fit values of a_l and ϵ_{nl} by fitting Equation (10) to the numerical results obtained from the Millennium Run N-body simulations (Springel et al. 2005), Lee & Pen (2008) demonstrated that for the galactic halos with masses in the range of $1.72 \leq M/(10^{11} h^{-1} M_\odot) \leq 10^2$ at redshifts $z \leq 0.5$, the second term proportional to $\tilde{\xi}(r)$ dominate the first term proportional to $\tilde{\xi}^2(r)$ in Equation (10).

3.2. Modeling the Anisotropic Tidal Effect

Although Lee & Pen (2008) found the linear scaling model, Equation (10), to work much better than the quadratic scaling model, Equation (9), Lee & Pen (2008) also detected a low but significant signal of the halo spin-spin correlation at distances as large as $r \geq 10 h^{-1} \text{Mpc}$, which could not be described by Equation (10) even with the best-fit parameters. The non-

zero value of $\eta(r)$ at $r \geq 10 h^{-1} \text{Mpc}$ turned out to be more significant especially at lower redshifts, $z \leq 0.5$, which implies that some additional nonlinear effect other than the non-Gaussianity must be responsible for the presence of this signal. To find an improved model that can describe the spin-spin correlations at $r \geq 10 h^{-1} \text{Mpc}$, we employ the extended model for the tidally induced spin alignments reviewed in Section 2.1.

Putting Equation (3) into the definition of $\eta(r)$, i.e., Equation (6), and using the same approximation made by Pen et al. (2000), we have

$$\eta(r) \approx \frac{9}{25} d_t^2 \langle \hat{T}_{ij} \hat{T}'_{ij} \rangle - \frac{1}{3} \quad (11)$$

$$\approx \frac{18}{25} d_t^2 \frac{\langle \tilde{T}_{ij} \tilde{T}'_{ij} \rangle}{\langle |\tilde{T}'|^2 \rangle} - \frac{1}{3}. \quad (12)$$

To see how the assumption of the isotropic tidal field leads $\langle \tilde{T}_{ij} \tilde{T}'_{ij} \rangle$ to be expressed in terms of $\tilde{\xi}(r)$, let us recall the following expression of $\langle \tilde{T}_{ij} \tilde{T}'_{kl} \rangle$ (Lee & Pen 2001):

$$\langle \tilde{T}_{ij} \tilde{T}'_{kl} \rangle = \langle T_{ij} T'_{kl} \rangle - \frac{1}{3} \delta_{kl} \langle T_{ij} T'_{nn} \rangle - \frac{1}{3} \delta_{ij} \langle T_{mm} T'_{kl} \rangle + \frac{1}{9} \delta_{ij} \delta_{kl} \langle T_{mm} T'_{nn} \rangle, \quad (13)$$

where

$$\begin{aligned} \langle T_{ij} T'_{kl} \rangle &= (\delta_{ij} \delta_{kl} + \delta_{ik} \delta_{jl} + \delta_{il} \delta_{jk}) \left[\frac{J_3(r)}{6} - \frac{J_5(r)}{10} \right] + \hat{r}_i \hat{r}_j \hat{r}_k \hat{r}_l \left[\xi(r) + \frac{5J_3(r)}{2} - \frac{7J_5(r)}{2} \right] \\ &+ (\delta_{ij} \hat{r}_k \hat{r}_l + \delta_{ik} \hat{r}_j \hat{r}_l + \delta_{il} \hat{r}_k \hat{r}_j + \delta_{jk} \hat{r}_i \hat{r}_l + \delta_{jl} \hat{r}_i \hat{r}_k + \delta_{kl} \hat{r}_i \hat{r}_j) \left[\frac{J_5(r)}{2} - \frac{J_3(r)}{2} \right], \end{aligned} \quad (14)$$

with

$$J_3(r) = \frac{3}{r^3} \int_0^r \xi(r') r'^2 dr'^2, \quad J_5(r) = \frac{5}{r^5} \int_0^r \xi(r') r'^4 dr'^4. \quad (15)$$

Equation (14) holds true only if the tidal field is isotropic. If $i = k$ and $j = l$, then all of the terms containing J_3 and J_5 in Equation (13) would vanish by symmetry, resulting in $\langle \tilde{T}_{ij} \tilde{T}'_{ij} \rangle$ expressed only in terms of $\xi(r)$. In the nonlinear regime, however, \mathbf{T} is far from being isotropic, the manifestation of which is nothing but the presence of the filamentary cosmic web (Bond et al. 1996). Assuming here that for the anisotropic \mathbf{T} , the terms containing J_3 and J_5 in the expression of $\langle \tilde{T}_{ij} \tilde{T}'_{ij} \rangle$ would not vanish, we propose the following fitting formula for $\eta(r)$:

$$\eta(r) \approx \frac{18}{25} d_t^2 \left[\tilde{\xi}(r) + g_3 \tilde{J}_3(r) - g_5 \tilde{J}_5(r) \right], \quad (16)$$

where $\tilde{J}_3 \equiv J_3/\sigma$, $\tilde{J}_5 \equiv J_5/\sigma$, while g_3 and g_5 are two adjustable parameters. As \mathbf{T} becomes more anisotropic, the second and third terms containing \tilde{J}_3 and \tilde{J}_5 , respectively, would become more dominant over the first term containing $\tilde{\xi}(r)$ in Equation (16). In other words, the values of g_3 and g_5 would increase as M and z decreases.

3.3. Numerical Tests

Now, we are going to numerically test the validity of Equations (11)-(16) using the same datasets from the ν^2 GC-H2 simulation that are described in Section 2.2. We first divide an interval $0 \leq r/(h^{-1}\text{Mpc}) \leq 20$ into short bins of the same length, Δr . Then, we compute the ensemble average of $\langle |\hat{\mathbf{s}} \cdot \hat{\mathbf{s}}'|^2 \rangle$ over all of the halo pairs whose values of r fall in each bin to numerically obtain $\eta(r)$ as defined in Equation (6). The one standard deviation of $\langle |\hat{\mathbf{s}} \cdot \hat{\mathbf{s}}'|^2 \rangle$ is also calculated as the associated errors. In a similar manner, we compute $\langle \hat{T}_{ij}(\mathbf{x}) \hat{T}'_{ij}(\mathbf{x} + \mathbf{r}) \rangle$ from the reconstructed tidal tensors and determine the mean value of d_t by Equation (4) from the measured values of $\hat{\mathbf{s}}$ and $\hat{\lambda}$ for each halo. Multiplying $\langle \hat{T}_{ij} \hat{T}'_{ij} \rangle$ by $9d_t^2/25$ and subtracting $1/3$ from it, we numerically obtain the RHS of Equation (11).

Figure 2 plots the numerically obtained $\eta(r)$ (filled circles) and compares it with the numerically obtained RHS of Equation (11) (brown solid lines) in the top panel. To show more clearly how $\eta(r)$ behaves at large distances, the bottom panel of Figure 2 plots the same as the top panel but in the logarithmic scale. As can be seen, except for the disagreement at the first bin from the left which corresponds to $r \leq 0.5 h^{-1}\text{Mpc}$, the RHS of Equation (11) describes quite well the overall amplitude and behavior of $\eta(r)$. Regarding the disagreement at the first bin, we suspect that it is likely caused by the resolution limit of the ν^2 GC-H2 simulation.

Now that the validity of Equation (11) is confirmed, we would like to verify the usefulness of our new formula, Equations (16). We determine the best-fit values of g_3 and g_5 by fitting Equation (16) to the numerically obtained $\eta(r)$ with the help of the χ^2 -statistics (see Table 1). Figure 3 plots Equation (16) with the best-fit parameters (red solid lines) and compares it with the numerical results (filled circles). We also fit Equations (9)-(10) to the numerical results by adjusting a_{nl} and $\{a_l, \epsilon_{\text{nl}}\}$, respectively, which are shown in Figure 3 (green and blue solid lines, respectively). As can be seen, Equation (9) that predicts the quadratic scaling of $\eta(r)$ with $\tilde{\xi}(r)$ grossly fails to describe $\eta(r)$ not only at large distances but everywhere. Equation (10) that predicts the linear scaling of $\eta(r)$ with $\tilde{\xi}(r)$ works better than Equation (9), but fails to match the non-vanishing tail of $\eta(r)$ at $r \geq 10 h^{-1}\text{Mpc}$, whose presence is believed to be induced by the anisotropic tidal effect. Whereas, Equation (16) matches the numerical results excellently in the whole range of r .

To see whether or not Equation (16) still works better than Equation (10) even for the case of $R_f \geq 5 h^{-1}\text{Mpc}$ and $M \geq 5 \times 10^{10} h^{-1} M_\odot$, we test it against the Small MultiDark Planck simulations (SMDPL) that has a larger simulation box of $L_{\text{box}} = 400 h^{-1}\text{Mpc}$ and a lower mass-resolution of $m_p = 9.63 \times 10^7 h^{-1} M_\odot$ than the ν^2 GC-H2 simulation (Klypin et al. 2016). Basically, we use the same dataset that Lee (2019) compiled and used, which contains the sample of the galactic halos with $0.5 \leq M/(10^{11} h^{-1} M_\odot) \leq 50$ at $z = 0$ and the values

of d_t measured at the location of each galactic halo from the alignments between the unit spin directions of the halos and the reconstructed local tidal field smoothed on the scale of $R_f = 5 h^{-1} \text{Mpc}$.

Repeating the same analysis described in the above but with the halo sample from the SMDPL, we numerically determine $\eta(r)$, to which Equations (9), (10) and (16) are fitted to find the best-fit values of their parameters (see Table 1). Regarding the value of d_t in Equation (16), we put the mean value averaged over the galactic halos in the sample from the SMDPL. Figure 4 plots the same as Figure 3 but with the sample from the SMDPL. As can be seen, the new formula, Equation (16), with the best-fit values of $\{g_3, g_5\}$ agrees best with the numerical results, even for the case of the higher mass halos and the much larger smoothing scale.

To see if the success of Equation (16) depends on the halo mass, we split the halo sample from the SMDPL into two subsamples: One contains the halos in the mass range of $0.5 \leq M/(10^{11} h^{-1} M_\odot) \leq 1$, while the rest of the halos with masses $1 \leq M/(10^{11} h^{-1} M_\odot) \leq 50$ belong to the other subsample. We perform the same analysis but with each subsample separately, the results of which are displayed in Figures 5-6. As can be seen, the best agreement is achieved by Equation (16) for both of the subsamples. For the subsample with higher-mass halos, however, we find the difference between Equations (16) and (10) to substantially diminish. This mass dependence of the fitting results indicates that the anisotropic tidal effect is less strong for the higher-mass halos and that the linear scaling of $\eta(r)$ with $\tilde{\xi}(r)$ is a fairly good approximation for the case of the halos with $M \geq 10^{11} h^{-1} M_\odot$.

We also examine the validity of Equation (16) at higher redshifts. Using the halos resolved at redshifts 0.2 and 0.4 from the SMDPL, we conducted the same analysis, the results of which are shown in Figures 7-8, respectively. At both of the redshifts, Equation (16) yields the best match to the numerically obtained $\eta(r)$. Note, however, that as $\eta(r)$ drops relatively faster with r at higher redshifts, the linear scaling, Equation (10), provides a good match to the numerical results at $z = 0.4$. Whereas, the original model suggested by Pen et al. (2000) turned out to be invalid at both of the redshifts. The best-fit values of the two parameters, g_3 and g_5 , of our new formula, Equation (16), for various cases of M , R_f and z are listed in Table 1. As can be seen, the value of g_5 drops with the increment of M and z much more rapidly than g_3 , which implies that the third term in Equation (16) is the most sensitive indicator of the anisotropic tidal effect.

4. Summary and Discussion

Using the high-resolution N-body simulations, we have determined the spin-spin correlation function, $\eta(r)$, of DM halos in a broad mass range of $0.01 \leq M/(10^{11} h^{-1} M_{\odot}) \leq 50$ at $z = 0$ and found it to decrease with the separation distance, r , much less rapidly than the rescaled two-point correlation function of the linear density field, $\tilde{\xi}(r)$, unlike the prediction of the previous model based on the tidal torque theory. However, the disagreement between the numerical results and the previous prediction has been shown to become smaller with the increment of z , almost vanishing at $z \geq 0.4$. Figuring out that the underlying assumption of the *isotropic* tidal field caused the disagreement, we have incorporated the anisotropic tidal effect into the previous model to derive a new formula with two fitting parameters for $\eta(r)$ expressed in terms of the integrals of $\tilde{\xi}(r)$. The new formula with the best-fit parameters has turned out to excellently match the numerical results in the broad range of the halo masses, describing especially well the behavior of $\eta(r)$ at large distances of $r \geq 10 h^{-1}\text{Mpc}$.

Although our new model deals with the low-mass galactic halos in the highly nonlinear regime, it requires no higher order nor nonlinear statistics. The halo spin-spin correlations can still be linked by our new model to the linear observables, the integrals of the rescaled linear density two-point correlation functions, $\tilde{J}_3(r)$ and $\tilde{J}_5(r)$, which in turn implies that our model would allow us to reconstruct the rescaled linear density two-point correlation by measuring the spin-spin correlation of the galactic halos. Since the large-scale tail of $\tilde{\xi}(r)$ is sensitively dependent on the nature and amount of DM, our model for $\eta(r)$ at large distances of $r \geq 10 h^{-1}\text{Mpc}$ could be used as a complementary probe of DM. Furthermore, our model for $\eta(r)$ is independent of the amplitude of $\xi(r)$, it has a potential to break the degeneracy between the power spectrum amplitude and the amount of dark matter.

To use our model for the halo spin-spin correlation function in practice as a probe of DM, however, the following issues must be addressed. The first issue is whether or not our formula for $\eta(r)$ is still valid even in the alternative non- Λ CDM cosmologies. High-resolution N-body simulations performed for alternative cosmologies would be required to examine this and to investigate how the best-fit parameters of our model depend on the background cosmology. The second issue is whether or not our model can also validly describe the directly observable spin-spin correlation of the luminous galaxies. Hydrodynamic simulations showed that the spin directions of the baryonic parts are aligned not with those of the entire DM halos but rather with those of the inner parts of the DM halos (e.g., Hahn et al. 2010). To apply our formula to describe the observed spin-spin correlation function of the luminous galaxies it will be necessary to examine whether or not the formula works well even when the spin directions are measured from the particles located in the inner central part of the DM halos.

The third issue is how to measure the spin directions of the galaxies as accurately as

possible from observations. For the cases of the giant late-type spiral galaxies whose position angles and axial ratios are available, the circular thin disk approximation has been conventionally employed to measure their spin directions (e.g., Lee & Erdogdu 2007; Lee 2011). For the case of the elliptical and dwarf galaxies, however, the same approximation cannot be used for the measurements of their spin directions since their shapes obviously deviate far from a circular thin disk. Detailed kinematic structures of the galaxies observed by a spectroscopic survey like MaNGA (“Mapping Nearby Galaxies at Apache Point Observatory”) (Bundy et al. 2015) may be useful to determine the three dimensional directions of the spin axes of those galaxies for which the conventional method fails (S. Kim private communication).

The fourth one is whether or not the same formula can be used to describe the galaxy spin-spin correlations measured in *redshift space* rather than in real space. In the original analysis of Pen et al. (2000), the linear density two-point correlation function was convolved with a Gaussian filter, $\exp[-r^2/(2\sigma_r^2)]$, to derive the spin-spin correlation function in redshift space, where $\sigma_r \sim 1.3 h^{-1}\text{Mpc}$ is the typical velocity dispersion of a giant spiral galaxy (Davis et al. 1997). However, since the galaxies with different types have different velocity dispersions, the errors associated with the values of σ_v are likely to contaminate the weak signals of the galaxy spin-spin correlations at $r \geq 10 h^{-1}\text{Mpc}$. A more elaborate method to recover the spin-spin correlation at large distances measured in redshift space will be necessary. Our future work is in the direction of resolving the above issues and testing the spin-spin correlation of the dwarf galaxies as a probe of DM.

I gratefully acknowledge the website, www.skiesanduniverses.org, for making the data from the $\nu^2\text{GC-H2}$ simulation accessible. The CosmoSim database used in this paper is a service by the Leibniz-Institute for Astrophysics Potsdam (AIP). The MultiDark database was developed in cooperation with the Spanish MultiDark Consolider Project CSD2009-00064. I gratefully acknowledge the Gauss Centre for Supercomputing e.V. (www.gauss-centre.eu) and the Partnership for Advanced Supercomputing in Europe (PRACE, www.prace-ri.eu) for funding the MultiDark simulation project by providing computing time on the GCS Supercomputer SuperMUC at Leibniz Supercomputing Centre (LRZ, www.lrz.de). The Bolshoi simulations have been performed within the Bolshoi project of the University of California High-Performance AstroComputing Center (UC-HiPACC) and were run at the NASA Ames Research Center.

I acknowledge the support of the Basic Science Research Program through the National Research Foundation (NRF) of Korea funded by the Ministry of Education (NO. 2016R1D1A1A09918491). I was also partially supported by a research grant from the NRF of Korea to the Center for Galaxy Evolution Research (No.2017R1A5A1070354).

REFERENCES

- Aragón-Calvo, M. A., van de Weygaert, R., Jones, B. J. T., & van der Hulst, J. M. 2007, *ApJ*, 655, L5
- Aslanyan, G., Price, L. C., Adams, J., et al. 2016, *Phys. Rev. Lett.*, 117, 141102
- Banik, I., & Zhao, H. 2018, *MNRAS*, 480, 2660
- Behroozi, P. S., Wechsler, R. H., & Wu, H.-Y. 2013, *ApJ*, 762, 109
- de Bernardis, P., Ade, P. A. R., Bock, J. J., et al. 2000, *Nature*, 404, 955
- Bett, P., Eke, V., Frenk, C. S., et al. 2007, *MNRAS*, 376, 215
- Bett, P. E., & Frenk, C. S. 2012, *MNRAS*, 420, 3324
- Bett, P. E., & Frenk, C. S. 2016, *MNRAS*, 461, 1338
- Biagetti, M. 2019, arXiv e-prints, arXiv:1906.12244
- Bland-Hawthorn, J., & Peebles, P. J. E. 2006, *Science*, 313, 311
- Bond, J. R., Kofman, L., & Pogosyan, D. 1996, *Nature*, 380, 603
- Bundy, K., Bershadsky, M. A., Law, D. R., et al. 2015, *ApJ*, 798, 7
- Carlesi, E., Mota, D. F., & Winther, H. A. 2017, *MNRAS*, 466, 4813
- Chisari, N. E., Dvorkin, C., Schmidt, F., et al. 2016, *Phys. Rev. D*, 94, 123507
- Codis, S., Pichon, C., Devriendt, J., et al. 2012, *MNRAS*, 427, 3320
- Codis, S., Gavazzi, R., Dubois, Y., et al. 2015, *MNRAS*, 448, 3391
- Codis, S., Pichon, C., & Pogosyan, D. 2015, *MNRAS*, 452, 3369
- Crittenden, R. G., Natarajan, P., Pen, U.-L., & Theuns, T. 2001, *ApJ*, 559, 552
- Davis, M., Miller, A., & White, S. D. M. 1997, *ApJ*, 490, 63
- Doroshkevich, A. G. 1970, *Astrofizika*, 6, 581
- Ganeshaiya Veena, P., Cautun, M., van de Weygaert, R., et al. 2018, *MNRAS*, 481, 414
- Hahn, O., Carollo, C. M., Porciani, C., & Dekel, A. 2007, *MNRAS*, 381, 41

- Hahn, O., Teyssier, R., & Carollo, C. M. 2010, MNRAS, 405, 274
- Hui, L. & Zhang Z. 2002, preprint [astro-ph/0205512]
- Hui, L., & Zhang, J. 2008, ApJ, 688, 742
- Ishiyama, T., Enoki, M., Kobayashi, M. A. R., et al. 2015, PASJ, 67, 61
- Kogai, K., Matsubara, T., Nishizawa, A. J., et al. 2018, JCAP, 2018, 014
- Klypin, A., Yepes, G., Gottlöber, S., et al. 2016, MNRAS, 457, 4340
- Lacerna, I., & Padilla, N. 2012, MNRAS, 426, L26
- Laigle, C., Pichon, C., Codis, S., et al. 2015, MNRAS, 446, 2744
- Lee, J., & Pen, U.-L. 2000, ApJ, 532, L5
- Lee, J., & Pen, U.-L. 2001, ApJ, 555, 106
- Lee, J., & Erdogdu, P. 2007, ApJ, 671, 1248
- Lee, J., & Pen, U.-L. 2008, ApJ, 681, 798
- Lee, J. 2011, ApJ, 732, 99
- Lee, J. 2019, ApJ, 872, 37
- Libeskind, N. I., Hoffman, Y., Forero-Romero, J., et al. 2013, MNRAS, 428, 2489
- Makiya, R., Enoki, M., Ishiyama, T., et al. 2016, PASJ, 68, 25
- Ntampaka, M., Trac, H., Cisewski, J., et al. 2017, ApJ, 835, 106
- Park, C.-G., & Ratra, B. 2018, arXiv e-prints, arXiv:1801.00213
- Paz, D. J., Stasyszyn, F., & Padilla, N. D. 2008, MNRAS, 389, 1127
- Pen, U.-L., Lee, J., & Seljak, U. 2000, ApJ, 543, L107
- Planck Collaboration, Ade, P. A. R., Aghanim, N., et al. 2014, A&A, 571, A16
- Porciani, C., Dekel, A., & Hoffman, Y. 2002, MNRAS, 332, 339
- Schmidt, F., Chisari, N. E., & Dvorkin, C. 2015, JCAP, 2015, 032
- Seo, H.-J., & Eisenstein, D. J. 2003, ApJ, 598, 720

- Silva, H. O., & Yunes, N. 2019, arXiv e-prints, arXiv:1902.10269
- Trowland, H. E., Lewis, G. F., & Bland-Hawthorn, J. 2013, ApJ, 762, 72
- Springel, V., White, S. D. M., Jenkins, A., et al. 2005, Nature, 435, 629
- Vittorio, N., Juszkiewicz, R., & Davis, M. 1986, Nature, 323, 132
- Welker, C., Devriendt, J., Dubois, Y., Pichon, C., & Peirani, S. 2014, MNRAS, 445, L46
- White, S. D. M. 1984, ApJ, 286, 38
- Yu, H.-R., Yu, Y., Motloch, P., et al. 2019, arXiv e-prints, arXiv:1904.01029
- Zel'dovich, Y. B. 1970, A&A, 5, 84
- Zhang, Y., Yang, X., Faltenbacher, A., et al. 2009, ApJ, 706, 747

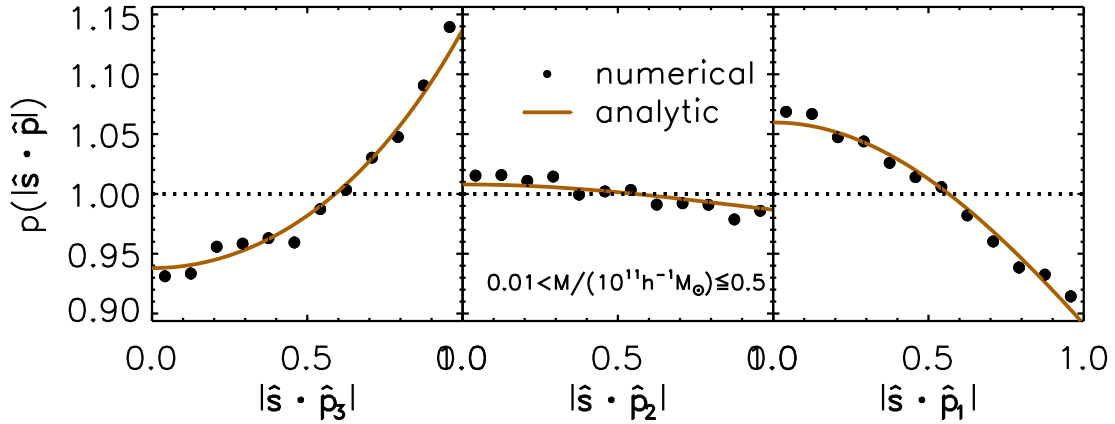


Fig. 1.— Probability density functions of the cosines of the angles of the unit spin vectors of the dwarf galactic halos with the third, second and first eigenvectors of the local tidal fields smoothed on the scale of $R_f = 0.5 h^{-1} \text{Mpc}$ (left, middle and right panels, respectively). In each panel, the numerical result with errors is displayed as filled circles while the analytic prediction from Equation (5) with $c_t = 0$ is plotted as brown solid line. The uniform probability density is also plotted as dotted line to show the statistical significance of the alignment signals in each panel.

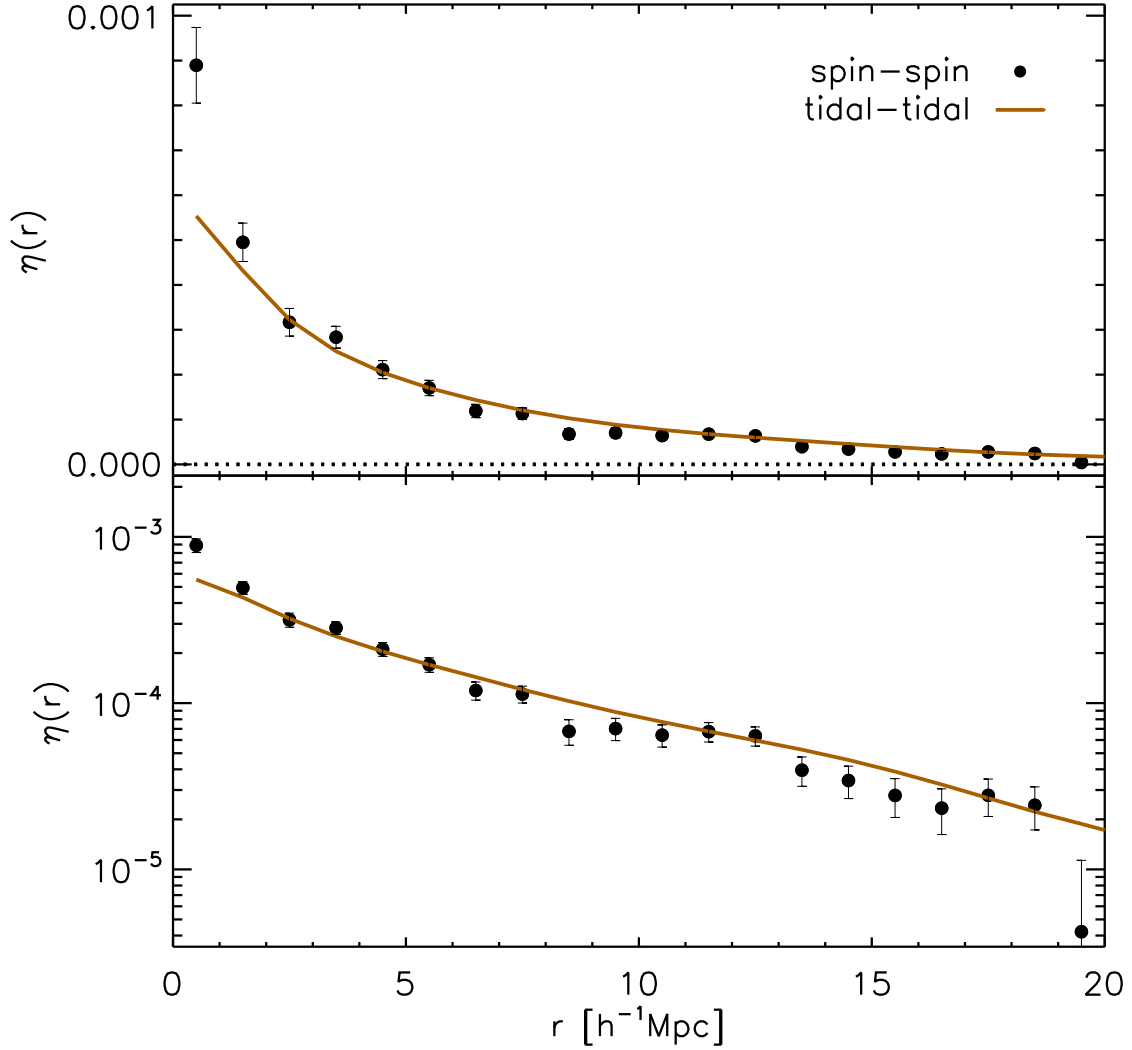


Fig. 2.— Correlations of the unit spin vectors between the neighbor dwarf galactic halos (filled circles) and the rescaled correlations of the unit traceless tidal tensors (brown solid line) between their positions as a function of the separation distance at $z = 0$ in the linear (top panel) and logarithmic scale (bottom panel).

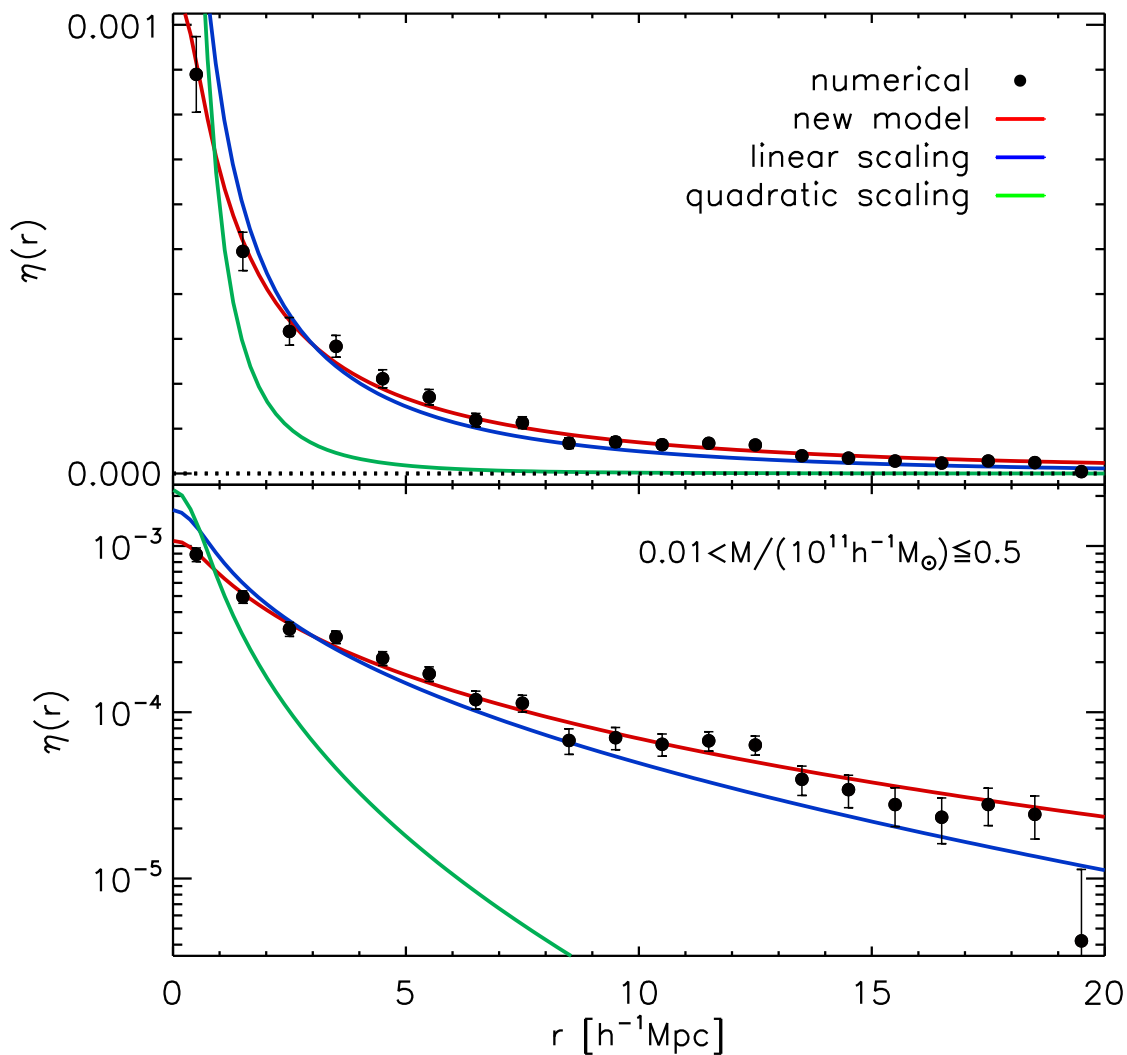


Fig. 3.— Comparison of the numerically obtained spin-spin correlations of the dwarf galactic halos (filled circles) with three different formulae, Equations (9), (10) and (16) with their best-fit parameters (green, blue and red solid lines, respectively.)

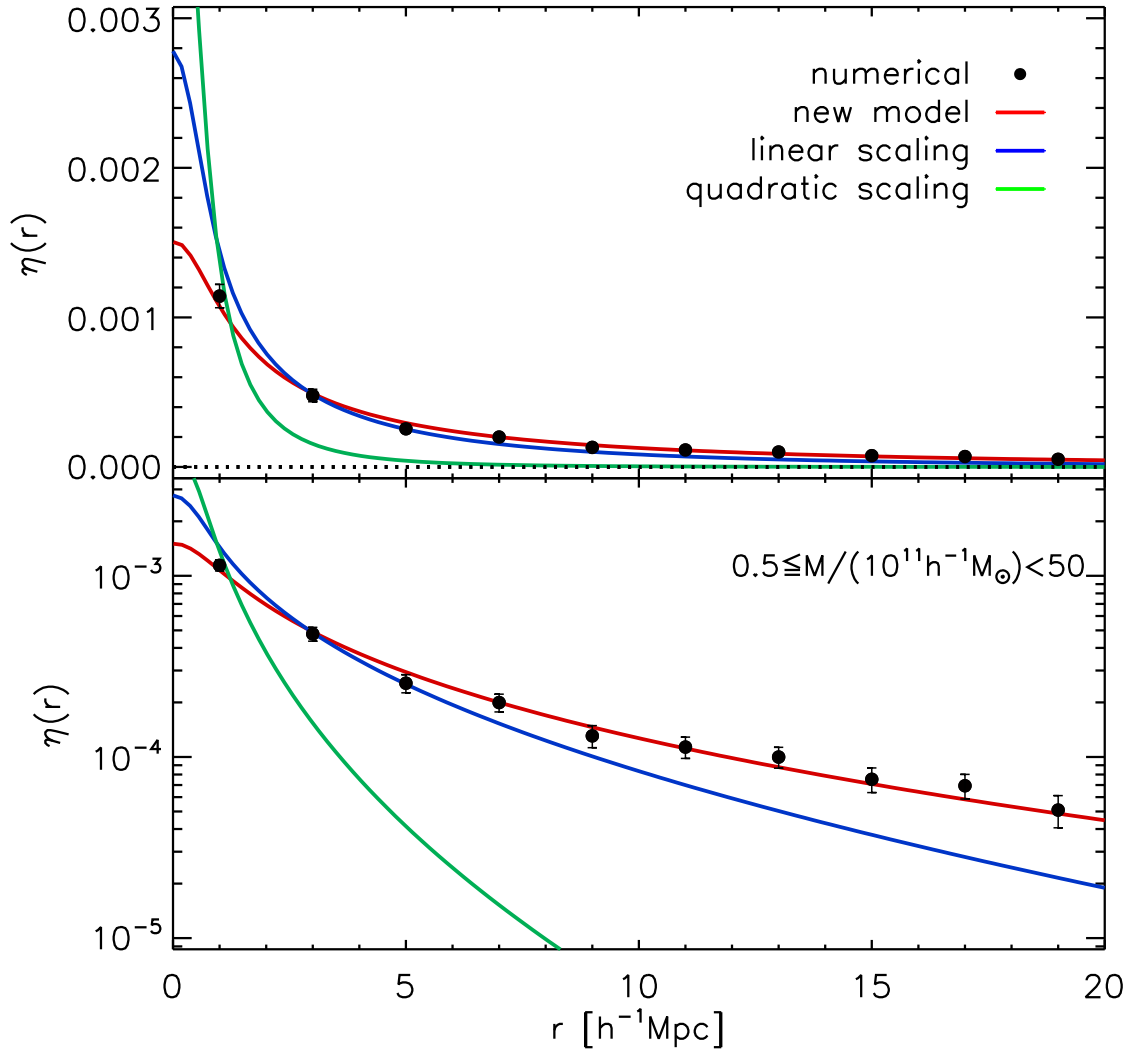


Fig. 4.— Same as Figure 3 but for the higher-mass galactic halos in the range of $0.5 \leq M / (10^{11} h^{-1} M_{\odot}) \leq 50$.

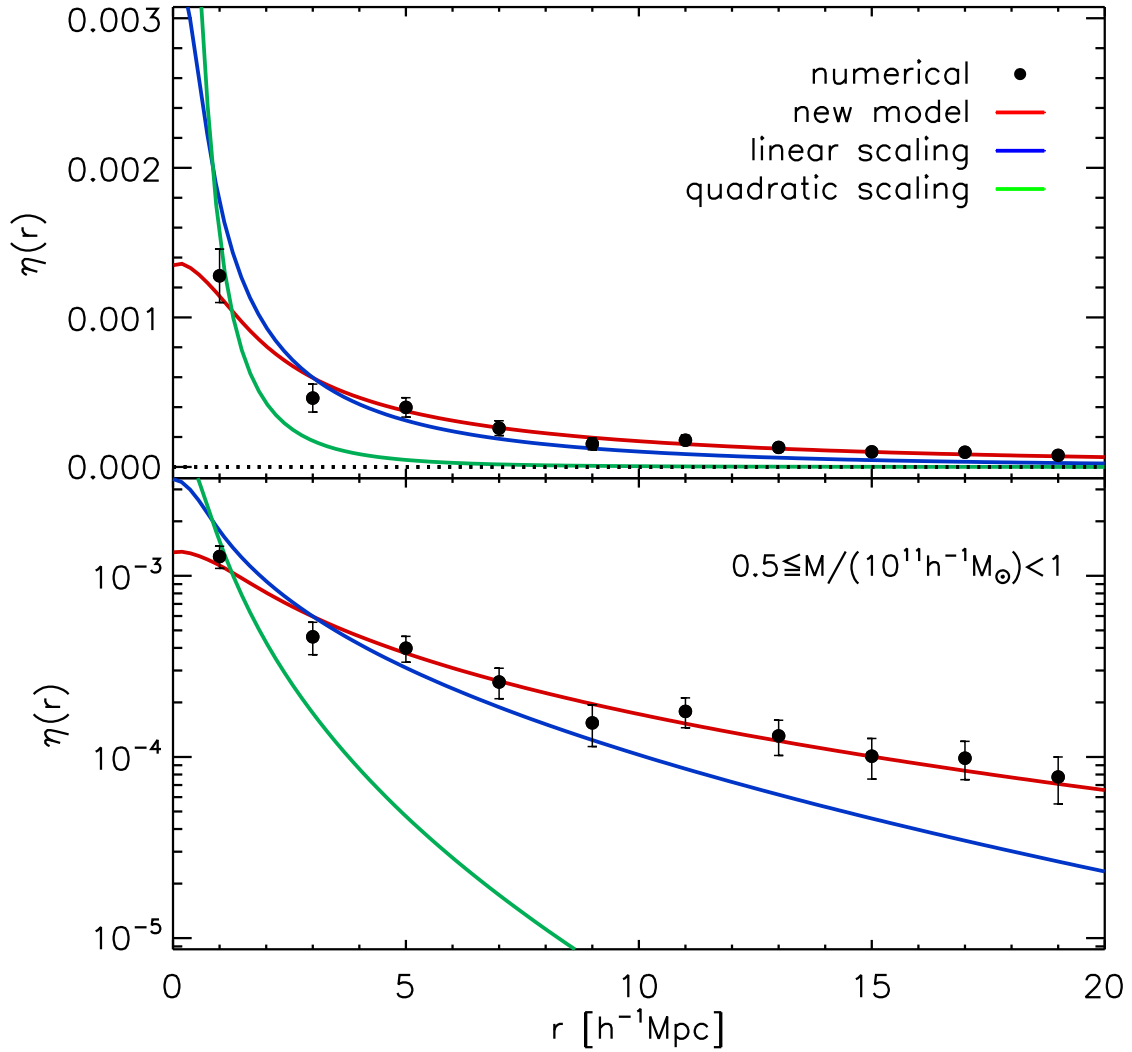


Fig. 5.— Same as Figure 4 but for the galactic halos in the narrower mass range of $0.5 \leq M/(10^{11} h^{-1} M_{\odot}) \leq 1$.

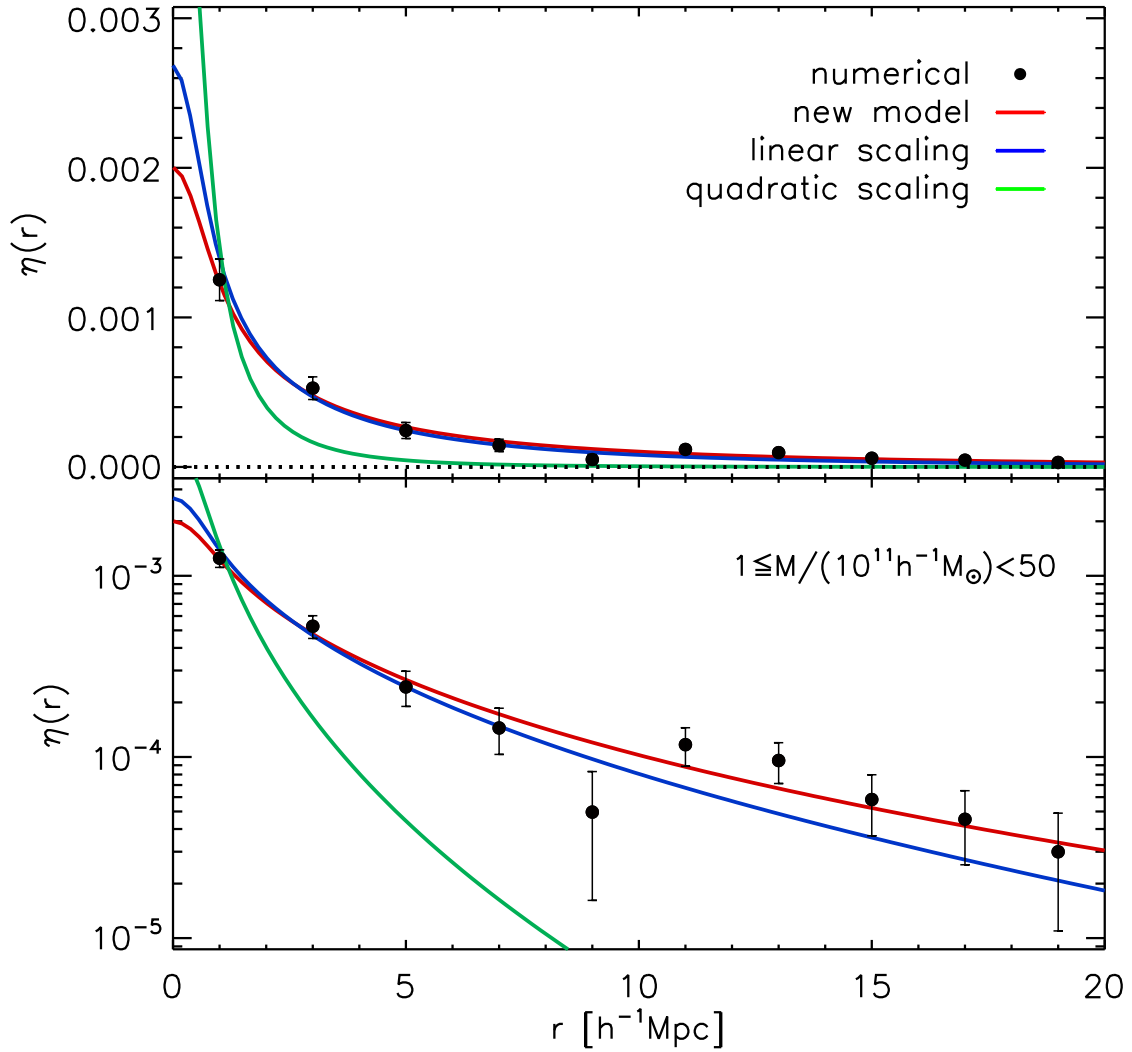


Fig. 6.— Same as Figure 5 but for the galactic halos in the higher mass range of $1 \leq M/(10^{11} h^{-1} M_{\odot}) \leq 50$.

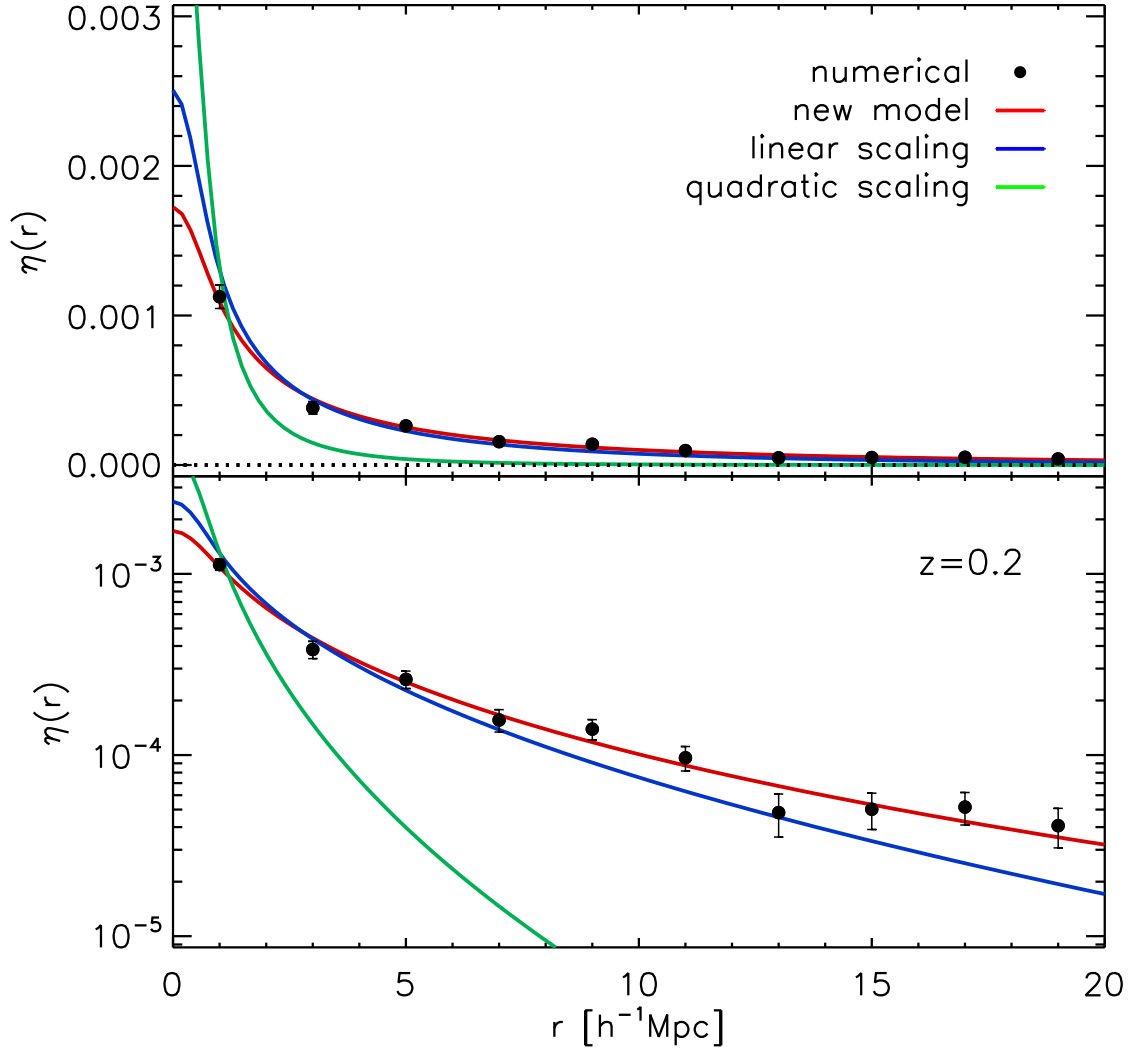


Fig. 7.— Same as Figure 4 but at $z = 0.2$.

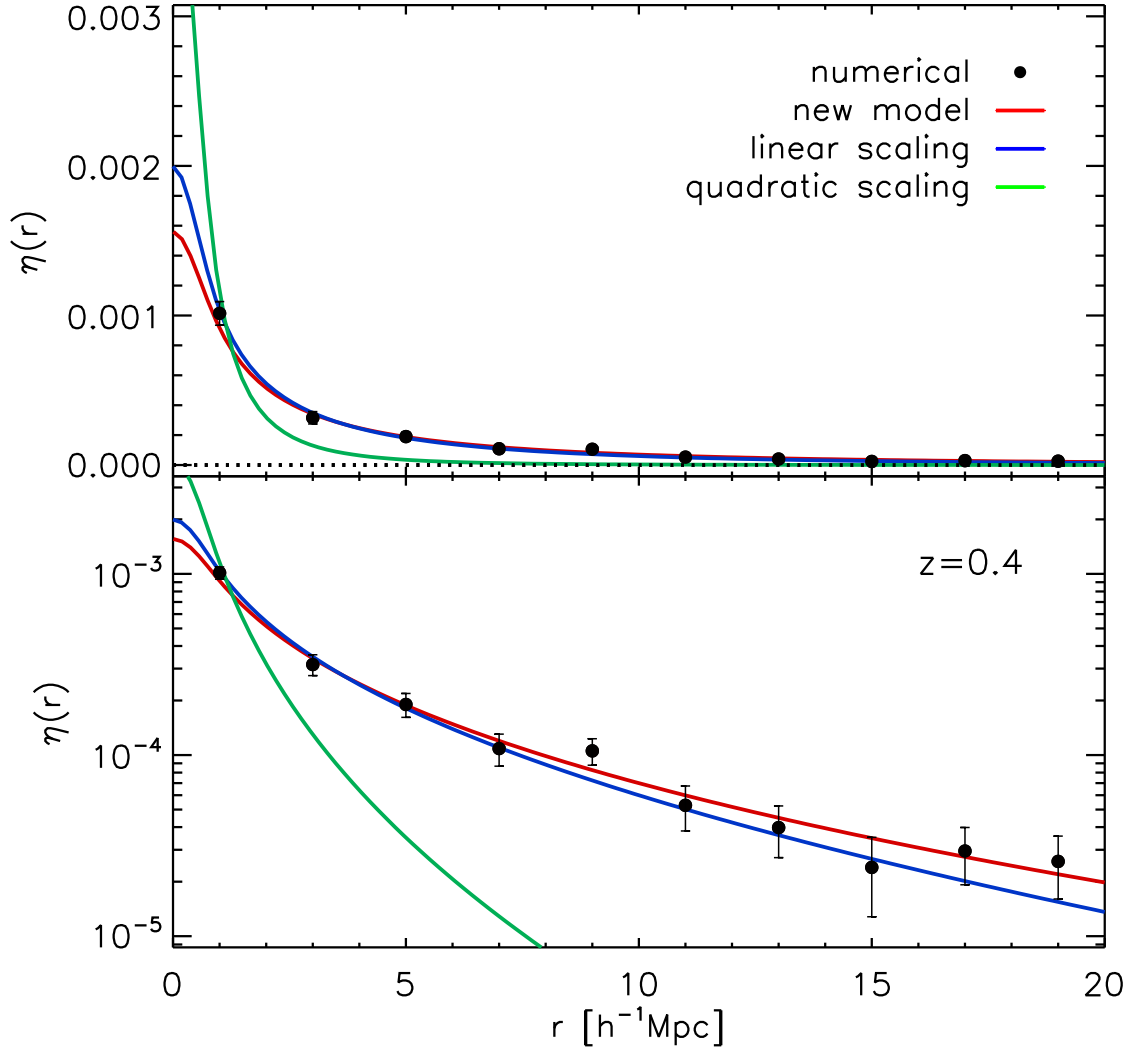


Fig. 8.— Same as Figure 4 but at $z = 0.4$.

Table 1. Best-fit Parameters for the Halo Spin-Spin Correlations

z	M ($10^{11} h^{-1} M_{\odot}$)	R_f ($h^{-1} \text{Mpc}$)	g_3	g_5
0.0	[0.01, 0.5)	0.5	2.1	2.3
0.0	[0.5, 50.0)	5.0	6.0	5.1
0.0	[0.5, 1.0)	5.0	8.3	8.0
0.0	[1.0, 50.0)	5.0	2.4	0.1
0.2	[0.5, 50.0)	5.0	3.0	1.8
0.4	[0.5, 50.0)	5.0	1.0	0.0